FUDMA Journal of Sciences (FJS)
ISSN online: 2616-1370
ISSN print: 2645 - 2944
Vol. 9 No. 8, August, 2025, pp 24 – 35
DOI: https://doi.org/10.33003/fjs-2025-0908-3695

COMBINED FLOW OF AN EXOTHERMIC FLUID WITH ELECTROKINETIC EFFECT OVER A MICROCHANNEL

[1]Muhammed Murtala Hamza, *[2]Godwin Ojemeri, [2]Mohammed Dago Maigemu, [2]Abdulsalam Shuaibu, [3]Idris Omakwu Usman, [2]Haruna Ishaya Germache and [2]Jeremiah Aaron Dazi

[1]Department of Mathematics, Faculty of Physical and Computing Sciences, Usmanu Danfodiyo University, P. M. B. 2346 Sokoto state, Nigeria.
[2]Department of Mathematics, College of Sciences, Federal University of Agriculture, Zuru, P. M. B. 28, Kebbi State, Nigeria.
[3]Brilliant Footsteps International Academy, Western Bypass, Sokoto.

*Corresponding authors' email: godwinojemeri@gmail.com

ABSTRACT
The steady state analysis of chemically reacting heat transfer problem of mixed convection flow in a vertical microchannel that is fully developed and embedded with electro-kinetic effect is performed in this article. The energy, electric potential, and momentum equations are solved in non-dimensional form under unequal wall zeta potentials, employing the homotopy perturbation method (HPM). The basic flow behavior of electric potentials, temperature, and velocity is investigated as a function of regulating parameters such as the Debye-Huckel parameter, mixed convection parameter, chemical reaction parameter, and rarefaction parameter. The findings are carefully examined and graphically represented in a number of illustrative plots. It was found that raising the levels of mixed convection, chemical reaction, and rarefaction parameters causes the fluid flow to escalate while the function of viscous heating term is to speed up the fluid temperature. Additionally, mounting values of Debye–Hückel parameter retards the electric potential in the micro-channel. Also, when the mixed convection, chemical reaction, electric potential, and streaming potential factors are ignored, the numerical computations of this findings are consistent with the previously published results.

Keywords: Electrokinetic effect, Exothermic fluid, Homotopy perturbation method (HPM), Microchannel, Mixed (Combined) convection, Streaming potential

INTRODUCTION

The modeling of mixed convection flow on stretching surfaces has piqued the interest and focus of researchers due to its emerging relevance in numerous realistic systems of immense applications in thermal energy storage, geothermal energy utilization, recoverable systems, petroleum reservoirs, metallurgy, polymer processing, geophysics, and other fields (Mandal *et al.* 2020). In the last decade, a good number of researches have been carried out in this field. Recently, Ojemeri *et al*. (2025) studied viscous Casson fluid flow in a mixed convection affected by exothermic chemical reaction across a vertical channel. Hindebu *et al*. (2022) analyzed the hydrodynamic and heat transfer problems of unsteady mixed convection flow of nanofluid in a micro-channel filled with porous material. Ajibade and Umar (2021) investigated the effects of viscous dissipation on a steady mixed convection Couette flow of heat generating/absorbing fluid. Hamza *et al.* (2019) discussed the combined impacts of the Soret effect, mixed convection, and radial magnetic field flow of viscous reactive fluid. Their computational results show that mixed convection and Soret parameters are seen to escalate the fluid velocity, while the radial magnetic field is observed to weaken the fluid flow. By utilizing the HAM, Daniel and Daniel (2015) carefully inspected the magnetohydrodynamics (MHD) mixed convection flow having a radiation influence through a stretching porous surface by utilizing the homotopy analysis method (HAM), while Jamaludin *et al.* (2020) explored the actions of heat emission/absorption on MHD mixed convection stagnation point in a hybrid nanofluid. They reported that the heat transfer of the conventional alumina/water nanofluid is higher than the copper–alumina water nanofluid with an increment in the heat source and sink parameter. Oztop *et al.* (2011) employed a finite volume technique to perform a hydro-magnetic mixed convection laminar fluid flow analysis in a lid-saturated enclosure heated by a corner heater under isothermal boundary situations having unequal lengths of bottom and right vertical surfaces. Attributable to their wide range of cooling purposes in material processing activities and manufacturing, micro heat pipes, space systems, micro-channel heat absorption, micro-jet impingement cooling, high-power density chips in supercomputers, and other electronics, micro-channel fluid and heat transfer flows have attracted a lot of interest in the past decade. Studying the flow pattern is becoming particularly critical for correct and proper modeling predictions since the bulk of these designs incorporate internal micro-channel flows (Al-Nimr and Khadrawi 2004, Jha *et al*. 2014a). Recent studies that looked at the effect of fluid flows on microgeometry in various physical situations have been published. In view of this, Hamza *et al*. (2025) recently investigated the significance of dusty fluid in unsteady fractional derivatives in Caputo-Fanrizio (CF) and Atangana-Baleanu in Caputo sense (ABC) in addressing heat transfer problem through a microchannel. Yale *et al.* (2023) explored the impacts of super-hydrophobicity and MHD on a viscous dissipative fluid in a slit microchannel coated with a superhydrophobic surface using a regular perturbation approach. Ojemeri and Onwubuya (2023) examined the impact of porosity in a viscous dissipative fluid affected by magnetic field along a microchannel. Onwubuya *et al.* (2024) recently evaluated the impact of viscous dissipation, porous medium and super-hydrophobicity on free convection of an electrically conducting fluid over an upstanding microchannel affected by an imposed magnetic field. The plates were alternatively heated and incorporated with heat source/sink effect. The implications of Hall current and the ion-slip condition on hydrodynamic free convection in a vertical micro-channel under the control of an induced magnetic field

was examined by Jha and Malgwi (2019a). Earlier on, Jha and Aina (2016) achieved exceptional precision in the solution of MHD free convection in a vertical micro-channel formed by two infinitely parallel electrically non-conducting plates. Jha *et al.* (2017) examined the effects of Hall current on hydro-magnetic free convection in a vertical micro-channel. Other works gave more insight into this field are provided in these references Chen and Weng (2005), Weng and Chen (2009), Buonomo and Manca (2012), and Jha and Aina (2015).

Due to its intriguing nature and potential applications in film vaporization in combustion chambers, cross-hatching on ablative surfaces, and transpiration cooling of re-entry vehicles and rocket boosters, the composition of flow patterns through viscous or chemically reactive fluids with MHD effects have gained increased attention over the years (Muthuraj and Srinivas, 2010). Frank–Kamenetskii (1969) was the first to present reactive viscous fluid modeling. The majority of lubricants used during engineering and industrial processes, including synthetic esters, hydrocarbon oils, polyglycols, and others, are reactive, as implied by Makinde (2008). In this context, Ojemeri *et al.* (2024) recently considered the significance of heat source/sink on a chemically reactive fluid through a microchannel. Ojemeri *et al.* (2023) carried out an analytical investigation of free convection on Soret and radial magnetic field of a chemically reactive fluid in an upright porous annulus. Ojemeri and Hamza (2022) reported a theoretical analysis of an Arrhenius kinetically driven heat generating/absorbing fluid in a microchannel. Hamza *et al*. (2022) carried out unsteady/steady chemically reacting fluid that is convectively heated, hydro-magnetic natural flow in a vertical channel imagined with a porous medium. While the unsteady state situation was determined by using a numerical scheme, the steady-state component was solved using the homotopy perturbation approach. The slip and Soret implications of free convection of a viscous, reactive fluid via a vertical porous cylinder having a radial magnetic field effect were explored by Ojemeri *et al*. (2019). The steady and unsteady effects of a fully developed free convection heat enhancement flow of reactive viscous fluids in a vertical porous pipe were reported by Ahmad and Jha (2015). They concluded that the rates of time-dependent and steady-state heat transfer across pipe layers increased over time. In a vertical channel and a tube, Jha *et al.* (2011a, 2011b) analytically and numerically investigated the consequences of a reactive viscous fluid in an unsteady free convection flow. It is concluded from their investigation that, growing values of the viscous heating term result in an improvement in the rate of heat transfer and shear stress on both channel surfaces.

Electro-kinetics concept involves removal of impurities in soil and the imposition of electric ions on flow creation, cardiac resuscitation, and battery cells creation or refilling (Arulanandam and Li 2000). This technique entails "the passage of a low voltage direct current electric field across the boundary of a fluid. "Scientists who were among the first to uncover the presence of electric body force in flow formulation are Reuss (1809), Probstein (1994). Reuss (1809) discovered that particles scattered in water migrate when electricity is applied continuously to porous clay. Debye–Hückel linearization (Debye and Hückel 1923) is a linearization technique that is commonly used in electroosmotic flow analysis. It is especially useful for minor EDL. Debye–Hückel linearization was used by Yang and Li (1998), who developed a numerical algorithm for electrokinetically controlled convectively heated liquid flows, and Jha and Oni (2019a), presented an analytical simulation for joint pressure and electroosmotic effect on the flow structure having an induced magnetic field employing the Debye–Hückel estimation. Later, Oni and Jha (2019) put forth a theoretical examination of steady and unsteady mixed convective flow formation towards a vertical micro-channel taking into account the influence of wall zeta potentials in the existence of an electric body force. Hamza *et al.* (2024a, 2024b) recently emphasized the impacts of electrokinetics through free and mixed convection flows affected by heat generation/absorption parameter and Helmholtz–Smoluchowski velocity along a superhydrophobic microchannel. Chakraborty *et al*. (2012), Jha and Oni (2018a, 2019b), Liechty *et al.* (2005), and Mukhopadhyay *et al.* (2009) have all contributed significantly to the analysis of coupled electro-kinetic and pressure gradient effects on flow generation in channels and microchannels.

Despite these interesting advancements, a critical gap remains in understanding the interaction of chemically reactive fluid, electrokinetic effect and mixed convection along a microchannel. However, this effect is particularly significant due its relevance in emerging MEMS, engineering sciences and lubrication industries; since most of the lubricants used in engineering and industrial processes, such as synthetic esters, hydrocarbon oils, polyglycols, and so on, are reactive. The ultimate goal of this research therefore is to analyze the consequences of a chemically reacting fluid and electro-osmotic effects on mixed convection flow past a vertical micro-channel affected by uneven wall zeta potentials. This paper is a modification of Jha *et al.* (2014a)'s work when the chemical reactant parameter, electro-kinetic and mixed convection effects are applied in the direction of the flow. This study is unique and novel in that it employs the homotopy perturbation technique to obtain an analytical representation of the effect of electro-kinetics caused by Electric Double Layer and chemically reacting fluid on heat transfer enhancement and flow characteristics in mixed convection flow in a vertical micro-channel experiencing unequal surface heating. The results obtained in this paper can create a better understanding of flow formations, improved heat transfer and decreased frictional force. Additionally, the findings from this research are intended to be useful in DNA analysis and sequencing systems, as well as to aid in the improvement of previous electro-osmotic flow research. This analysis is also inspired by the high demand for diverse industrial working fluids and previous presentations on the importance of Arrhenius energy and exothermic chemical reaction to biotechnology, thermal sciences, chemical engineering, food processing, and others.

Problem Formulation

We look at a steady fully developed mixed convective Arrhenius-controlled fluid in a vertical micro-channel that has a wideness of b, which is subjected to uneven wall electric potentials ξ_1 and ξ_2 and temperatures T_1 and T_2 at the micro-channel walls (y = 0 and y = H). A density differential occurs as a result of the disparity in wall temperatures, resulting in a natural convection flow in the micro-channel. An EDL is formed when a fluid phase having negative or positive ions comes into contact with a negatively or positively charged solid surface (Mala et al. 1997). Ion convection effects are minimal in the EDL because the charge distribution follows the Boltzmann distribution. In this present work, as illustrated in Figure 1, fluid motion is assumed to be induced by a combination of electric body force and Arrhenius kinetics.

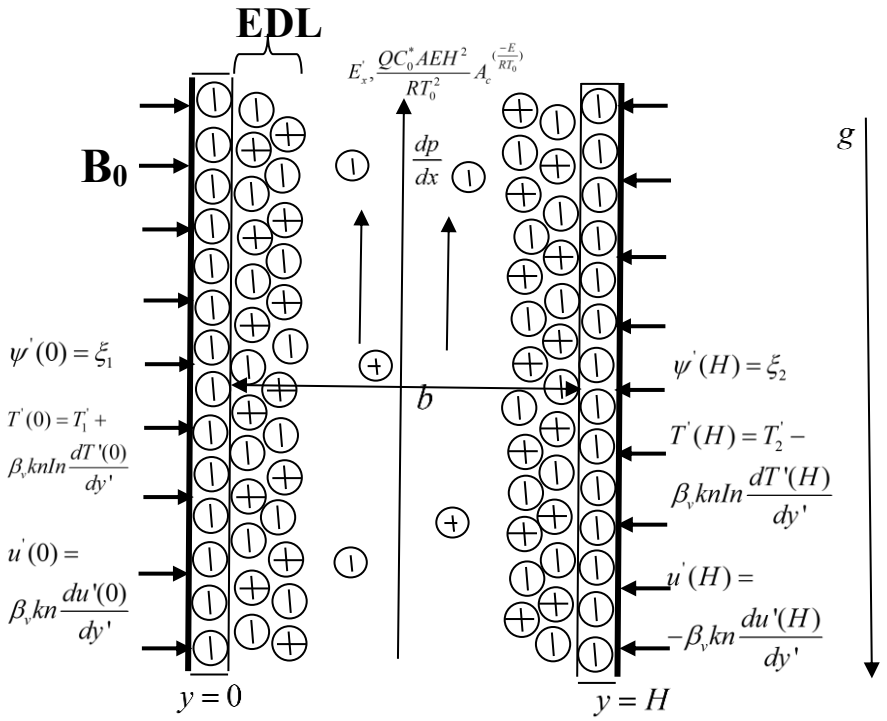

Figure 1: Schematic Diagram of the flow system

Hunter (1981) derives the electrical potential gradients from the Poisson-Boltzmann equation using the assumption above:

$$\nabla^2\phi = -\frac{\rho_c}{\varepsilon'} \quad (1)$$

Where $\phi$is the result of a composition of the outwardly imposed field$\Phi$and the EDL potential $\psi, (\phi = \psi + \Phi)$ and Mukhopadhyay *et al*. (2009) defines *ρc* as the charge density per unit of volume of a symmetric electrolyte.

$$\rho_c = -2FzC_0\, sinh(\frac{zF\psi\prime}{R\prime T}) \quad (2)$$

The fully developed region's external potential gradient runs in the direction of axis

$\Phi = \Phi(x)$ and $\psi' = \psi'(y')$only as:

$$\frac{d^2\psi\prime}{dy\prime^2} = \frac{2FzC_0}{\varepsilon} sinh(\frac{2F\psi\prime}{R\prime T}) \quad (3)$$

Subjected to $\psi'(0) = \xi_1, \psi'(H) = \xi_2$ (4)

applying the Boussinesq approximation which is denoted as:

$$\rho = \rho_0[1 - \beta(T' - T_0^1)] \quad (5)$$

$$u_s = -\frac{2-\sigma_v}{\sigma_v}\lambda\frac{\partial u}{\partial z}\Big|_{z=b} \quad (6)$$

$$T_s - T_w = -\frac{2-\sigma_v}{\sigma_v}\frac{2\gamma}{\gamma+1}\frac{\lambda}{Pr}\frac{\partial T}{\partial z}\Big|_{z=b} \quad (7)$$

Under the assumption of the Boussinesq approximation, and following Ojemeri and Hamza (2022) and Hamza *et al*. (2022), the controlling momentum and energy equations in dimensional form that describe the flow formation and temperature distributions can be written as:

$$\upsilon\frac{\partial^2 u\prime}{\partial y\prime^2} - \frac{\mu_e B_0' u\prime}{\rho} - \rho_c E_x' + \rho_0 g\beta(T' - T_0) = \frac{1}{p}\frac{\partial P}{\partial x} \quad (8)$$

$$\frac{\partial^2 T\prime}{\partial y\prime^2} + \frac{QC_0^* A}{k} e^{(\frac{-E}{RT\prime})} = 0 \quad (9)$$

$$u'(y') = \frac{2-\sigma_v}{\sigma_v}\lambda\frac{\partial u'}{\partial y'}, T'(y') = T_2 + \frac{2-\sigma_v}{\sigma_v}\frac{2\gamma}{\gamma+1}\frac{\lambda}{Pr}\frac{\partial T'}{\partial y'} at\ y' = 0 \quad (10)$$

$$u'(y') = -\frac{2-\sigma_v}{\sigma_v}\lambda\frac{\partial u'}{\partial y'}, T'(y') = T_1 - \frac{2-\sigma_v}{\sigma_v}\frac{2\gamma}{\gamma+1}\frac{\lambda}{Pr}\frac{\partial T'}{\partial y'} at\ y' = H \quad (11)$$

The non-dimensional quantities used are:

$$U = \frac{u'}{u_0}, Y = \frac{y'}{H'}, X = \frac{x'}{Re\,H'}, \psi = \frac{z'F\psi'}{R'T}, , \theta = \frac{T-T_0}{T_1-T_0}, \lambda = \frac{QC_0^* AEH^2}{RT_0^2} e^{\left(\frac{-E}{RT_0}\right)}, M^2 = \frac{\sigma B_0^2 H^2}{\rho v},$$

$$\varepsilon = \frac{RT_0}{E}, \kappa = \frac{H}{\lambda_D}, \lambda_D = \left[\frac{\varepsilon\prime R\prime T}{2F^2 z\prime^2 C_0}\right]^{\frac{1}{2}}, \xi_1^* = \frac{z\prime F\xi_1}{R\prime T}, \xi_2^* = \frac{z\prime F\xi_2}{R\prime T}, \Gamma = \frac{\varepsilon R\prime T\xi_1}{z\prime F\rho_0 v^2}, E_x = \frac{E_x' H}{\xi},$$

$$u_0 = \frac{\rho g\beta(T_1-T_0)H^2}{\mu}, Gr = \frac{g\beta(T_2'-T_0')H^3}{v^2}, Re = \frac{Hu_0}{v}, P = \frac{p}{\rho u_0^2} \quad (12)$$

Using Eqn. (12), the governing equation for the electric potential in non-dimensional state is:

$$\frac{d^2\psi}{dy^2} - \kappa^2\, sinh\,\psi = 0 \quad (13)$$

The ratio of the ions' electrical potential to thermal energy is also assumed to be less than one $\left(\frac{|zF\psi|}{|RT|} < 1\right)$(Liechty *et al.* 2005), allowing Eq. (13) to be linearized employing the Taylor approximation about the first term. As a result, the potential is assumed to be minimal to the extent that Debye–Hückel linearization is useful, and Eqn. (13) is renamed (Debye and Hückel linearization 1923).

$$\frac{d^2\psi}{dy^2} - \kappa^2\psi = 0 \quad (14)$$

$$\psi(0) = \xi_1^*\psi(1) = \xi_2^* \quad (15)$$

inserting the dimensionless parameters described in Eqn (12) into Eqns. (8–11), the velocity and temperature gradients in nondimensional state becomes:

$$\frac{d^2U}{dy^2} - M^2U - E_x\kappa^2\Gamma\psi + \frac{Gr}{Re}\theta = A \quad (16)$$

$$\frac{d^2\theta}{dy^2} + \lambda e^{\frac{\theta}{1+\varepsilon\theta}} = 0 \quad (17)$$

The following are the boundary conditions at the walls;

$$\left.\begin{aligned} U(y) = \beta_v Kn\frac{dU}{dy},\ \theta(Y) = \xi + \beta_v KnIn\frac{d\theta}{dy}, at \quad y = 0 \\ U(y) = -\beta_v Kn\frac{dU}{dy},\ \theta(Y) = 1 - \beta_v KnIn\frac{d\theta}{dy}, at\ y = 1 \end{aligned}\right\} \quad (18)$$

Where ψ is the electric potential, ξ_2^*, ξ_1^* are the unequal wall zeta potentials, M is the magnetic field intensity, κ is the Debye–Hückel parameter, $\Gamma$is the magnitude of electrokinetic effect, $E_x$is the streaming potential, $\frac{Gr}{Re}$= (Gre) is the mixed convection parameter, A =$\frac{dP}{dX}$ is the pressure gradient and λ is essentially the viscous heating parameter known as Frank–Kamenetskii parameter. It is important to mention that, in the expansion of heat source term $\lambda(1+\varepsilon\theta)^m e^{\frac{\theta}{1+\varepsilon\theta}}$, the Arrhenius heating case (i.e. when m = 0) was considered in this study.

Solution Procedure

To solve the governing dimensionless equations, we used the homotopy perturbation approach and constructed a convex homotopy on Eqns (14-18), we have:

$$H(\theta,\psi) = (1-p)\frac{d^2\psi}{dy^2} - p[\kappa^2\psi] = 0 \quad (19)$$

$$H(U,p) = (1-p)\frac{d^2U}{dy^2} - p\left[M^2U + E_x\kappa^2\Gamma\psi - \frac{Gr}{Re}\theta + A\right] = 0 \quad (20)$$

$$H(\theta,p) = (1-p)\frac{d^2\theta}{dy^2} + p\left[\lambda e^{\frac{\theta}{1+\varepsilon\theta}}\right] = 0 \quad (21)$$

We assume that the solutions of ψ, U and θ is in the infinite series form as follows:

$$\left.\begin{aligned}\psi(y) &= v_0 + pv_1 + p^2v_2 + \dots\\ \theta(y) &= \theta_0 + p\theta_1 + p^2\theta_2 + \dots\\ U(y) &= u_0 + pu_1 + p^2u_2 + \dots\end{aligned}\right\} \quad (22)$$

and substituting equation (22) into Eqns (19-21), and comparing the coefficient of similar powers p, we have the sets of differential equations with their corresponding boundary conditions as follows:

$$p^0:\begin{cases}\frac{d^2v_0}{dy^2} = 0 & (23)\\ \frac{d^2\theta_0}{dy^2} = 0 & (24)\\ \frac{d^2u_0}{dy^2} = 0 & (25)\end{cases}$$

The transformed boundary conditions now becomes

$$\left.\begin{aligned}v_0 &= \xi_1^*\\ \theta_0 &= \xi + \beta_v KnIn\frac{d\theta_0}{dy}\\ u_0 &= \beta_v Kn\frac{du_0}{dy}\end{aligned}\right\} at\ y = 0 \quad (26)$$

$$\left.\begin{aligned}v_0 &= \xi_2^*\\ \theta_0 &= 1 - \beta_v KnIn\frac{d\theta_0}{dy}\\ u_0 &= -\beta_v Kn\frac{du_0}{dy}\end{aligned}\right\} at\ y = 1 \quad (27)$$

$$p^1:\begin{cases}\frac{d^2v_1}{dy^2} = \kappa^2 v_0 & (28)\\ \frac{d^2\theta_1}{dy^2} + \lambda(1+\theta_0+(2-\varepsilon)\theta_0^2) = 0 & (29)\\ \frac{d^2u_1}{dy^2} - M^2u_0 - E_x\kappa^2\Gamma v_0 + \frac{Gr}{Re_0}\theta_0 - A = 0 & (30)\end{cases}$$

The transformed boundary conditions now become

$$\left.\begin{aligned}v_1 &= 0\\ \theta_1 &= \beta_v KnIn\frac{d\theta_1}{dy}\\ u_1 &= \beta_v Kn\frac{du_1}{dy}\end{aligned}\right\} at\ y = 0 \quad (31)$$

$$\left.\begin{aligned}v_1 &= 0\\ \theta_1 &= -\beta_v KnIn\frac{d\theta_1}{dy}\\ u_1 &= -\beta_v Kn\frac{du_1}{dy}\end{aligned}\right\} at\ y = 1 \quad (32)$$

$$p^2:\begin{cases}\frac{d^2v_2}{dy^2} = \kappa^2 v_1 & (33)\\ \frac{d^2\theta_2}{dy^2} + \lambda(\theta_1 - 2\varepsilon\theta_1\theta_0 + 4\theta_1\theta_0) = 0 & (34)\\ \frac{d^2u_2}{dy^2} - M^2u_1 - E_x\kappa^2\Gamma v_1 + \frac{Gr}{Re_1}\theta_1 = 0 & (35)\end{cases}$$

The transformed boundary conditions now become

$$\left.\begin{aligned}v_2 &= 0\\ \theta_2 &= \beta_v KnIn\frac{d\theta_2}{dy}\\ u_2 &= \beta_v Kn\frac{du_2}{dy}\end{aligned}\right\} at\ y = 0 \quad (36)$$

$$\left.\begin{aligned}v_2 &= 0\\ \theta_2 &= -\beta_v KnIn\frac{d\theta_2}{dy}\\ u_2 &= -\beta_v Kn\frac{du_2}{dy}\end{aligned}\right\} aty = 1 \quad (37)$$

The solutions of $v_0, v_1, v_2\dots, \theta_0, \theta_1, \theta_2\dots and u_0, u_1, u_2\dots$have been derived as follows:

$$v_0 = D_0y + D_1 \quad (38)$$

$$v_1 = \kappa^2\left[(\xi_2^* - \xi_1^*)\frac{y^3}{6} + \xi_1^*\frac{y^2}{2}\right] + D_2y + D_3 \quad (39)$$

$$v_2 = \kappa^2\left[(\xi_2^* - \xi_1^*)\frac{y^5}{120} + \xi_1^*\frac{y^4}{24}\right] + \kappa^2D_2\frac{y^3}{6} + \kappa^2D_3\frac{y^2}{2}D_4y + D_5 \quad (40)$$

$$\theta_0 = A_0 + A_1y \quad (41)$$

$$\theta_1 = -\lambda[\ \frac{y^2}{2} + A_0\frac{y^2}{2} + A_1\frac{y^3}{6} + (2-\varepsilon)(A_0^2\frac{y^2}{2} + A_0A_1\frac{y^3}{3} + A_1^2\frac{y^4}{12})\ ] + A_3y + A_2 \quad (42)$$

$$\theta_2 = -(4\lambda - 2\varepsilon\lambda)\left[\lambda\{A_0\frac{y^4}{24} + A_0^2\frac{y^4}{24} + A_0A_1\frac{y^5}{120} + (2-\varepsilon)(A_0^3\frac{y^4}{24} + A_0^2A_1\frac{y^5}{60} + A_0A_1^2\frac{y^6}{360})\ \} + A_0A_3\frac{y^3}{6} + A_0A_2\frac{y^2}{2} - \lambda\left\{A_1\frac{y^5}{40} + A_0A_1\frac{y^5}{40} + A_1^2\frac{y^6}{180} + (2-\varepsilon)(A_0^2A_1\frac{y^5}{40} + A_0A_1^2\frac{y^6}{60} + A_1^3\frac{y^7}{504})\ \} + A_3A_1\frac{y^4}{12} + A_2A_1\frac{y^3}{6}\ ] + \lambda^2\left\{\frac{y^4}{24} + A_0\frac{y^4}{24} + A_1\frac{y^5}{120} + (2-\varepsilon)(A_0^2\frac{y^4}{24} + A_0A_1\frac{y^5}{60} + A_1^2\frac{y^6}{360})\ \} + \lambda(A_3\frac{y^3}{6} + A_2\frac{y^2}{2}) + A_5y + A_4 \quad (43)$$

$$u_1 = E_x\kappa^2\Gamma\left(D_0\frac{y^3}{6} - D_1\frac{y^2}{2}\right) - \frac{Gr}{Re}\left(A_0\frac{y^2}{2} + A_1\frac{y^3}{6}\right) + A\frac{y^2}{2} + CC_1y + CC_2 \quad (44)$$

$$u_2 = M^2E_x\kappa^2\Gamma\left(D_0\frac{y^3}{6} - D_1\frac{y^2}{2}\right) + M^2\frac{Gr}{Re_0\frac{y^4}{24_1}\frac{y^5}{120}\frac{y^4}{24_1}\frac{y^3}{6_2}\frac{y^2}{2}}E_x\kappa^4\Gamma\left[(\xi_2^* - \xi_1^*)\frac{y^5}{120} + \xi_1^*\frac{y^4}{24}\right] + E_x\kappa^2\Gamma\left(D_2\frac{y^2}{2} + D_3y\right) + \lambda\frac{Gr}{Re\left\{\frac{y^4}{24_0}\frac{y^4}{24_1}\frac{y^5}{120}\right.}(2-\varepsilon)(A_0^2\frac{y^4}{24} + A_0A_1\frac{y^5}{60} + A_1^2\frac{y^6}{360})\ \} - \frac{Gr}{Re\left(A_3\frac{y^3}{6} + A_2\frac{y^2}{2}\right)_{3_4}} \quad (45)$$

Setting p=1, from Eqn (22), the solutions of ψ, U and θ in the approximate form becomes

$$\psi(y) = v_0 + v_1 + v_2 + \dots \quad (46)$$

$$\theta(y) = \theta_0 + \theta_1 + \theta_2 + \dots \quad (47)$$

$$U(y) = u_0 + u_1 + u_2 + \dots \quad (48)$$

The series in Eqns (46-48) typically converges even for few terms. On the other hand, the nonlinear operator determines the rate of convergence. Ayati and Biazar (2015) assert that only a few terms of the homotopy perturbation procedure estimation can be used to get an approximative solution when the homotopy perturbation converges to the series solution.

For a steady fully developed channel flow, to calculate the pressure gradient $A = \frac{dP}{dx}$ of the flow assuming a uniform mass flux Q, we integrate the velocity (U) from 0 to 1 with respect to y:

$$u_0 = \frac{\int_0^1 U(y)dy}{\int_0^1 dy} = Q \quad (49)$$

So that

$$\frac{dP}{dx} = \frac{Q+w37-w36-w8(\frac{1}{2}+B_v kn)-w38-w39-w40-w42-w44-w45-w46+w47-w34(\frac{1}{2}+B_v kn)}{\frac{1}{6}-w9(\frac{1}{2}+B_v kn)+\frac{M^2}{120}-w41-w43+w35(\frac{1}{2}+B_v kn)} \quad (50)$$

The turning point of the velocity (U) is used to determine the values of the mixed convection parameter Gre (critical values) at which the fluid's velocity yields a negative value (reverse flow) at the stationary plate y=1, then the critical values are obtained from $\left.\frac{du}{dy}\right|_{y=1} = 0$. The critical values for the different flow parameters are demonstrated in Table 2.

We obtained the frictional force (τ) on both walls as

$$sk\,inf\,r\,iction(\tau_0) = \left.\frac{dU}{dy}\right|_{y=0} \quad (51)$$

$$sk\,inf\,r\,iction(\tau_1) = \left.\frac{dU}{dy}\right|_{y=1} \quad (52)$$

The heat transfer rate at both surfaces are derived as:

$$Nu_0 = \frac{qb}{(T_1-T_0)k} = \left.\frac{d\theta}{dy}\right|_{y=0} \quad (53)$$

$$Nu_1 = \frac{qb}{(T_1-T_0)k} = \left.\frac{d\theta}{dy}\right|_{y=1} \quad (54)$$

The constants used are all described in the appendices section

RESULTS AND DISCUSSION

In order to see the physical impacts of various regulating parameters mixed convection $\frac{Gr}{Re}$= Gre, chemically reacting fluid λ, rarefaction $\beta_v Kn$, Debye–Hückel parameter κ, electric double layer EDL, streaming potential E_x, wall zeta potentials ξ_2^*, on flow pattern and heat transmission, graphs and tables are provided to assist in understanding the impact of various relevant parameters on flow generation and heat transmission in the vertical micro-channel. Throughout this article, the wall ambient temperature ratio parameter ($\xi\xi$), which assesses the level of asymmetric wall heating, will be set to (ξ= 0, ξ = 1), taken over the range 0.0 ≤ ($\xi\xi$) ≤ 1.0, and the Debye–Hückel parameter , which varies inversely to electric double layer EDL size, will be set to 0.5 ≤ κ ≤ 2. The current article's reference values are$\xi = \xi_1^* = \xi_2^* = 1$, κ = 0.5, Γ= 2.0.These numbers were carefully chosen to solve a physical problem in micro-fluidics.

Table 1 shows the necessary pressure gradient to push the flow to a specified mass flux, and Table 2 displays the critical Gre values required to achieve flow reversal close to the stationary plate. Table 3 and 4 provide descriptions of skin friction and heat transfer rates at the fluid-plate contact.

Figure 2 demonstrate the actions of Gre and (ξ_2^*) at a constant pressure gradient on the velocity distribution. An escalation in the fluid flow is established for higher levels of Gre and this effect is stronger at (ξ_2^*= 1.0) than at (ξ_2^*= 0.0). Figures 3 and 4 depict the effect of ($\beta_v Kn$) and (λ) on the temperature distributions respectively in two different wall-ambient temperature differential ratios: (ξ=0 indicates that one wall is heated while the other is not, and ξ=1 indicates that both walls are heated.) It is seen that as the values of ($\beta_v Kn$) and (λ) increase, so does the temperature jump. The actions of electric potential for various values of κ andξ_2^* is demonstrated in Figure 5. By applying uneven zeta-potential to the micro-channel walls, the maximum electric potential is achieved. Furthermore, growing values of κ suppresses the potential of the micro-electric channel. When we look at this image again, we can see that increasing the Debye–Hückel parameter (κ) eliminates the EDL effect. This may be because increasing κ causes the EDL thickness to decrease, lowering the electric potential in the micro-channel. Figures 6 explain the velocity deviations for various levels of the rarefaction parameter ($\beta_v Kn$). According to a detailed examination, increasing the ($\beta_v Kn$) level improves the velocity slip at the wall. The velocity profile is also found to be higher with zeta potential (ξ_2^*= 1.0) than with zeta potential (ξ_2^*= 0.0). The EDL's streaming potential is an important physical property in electro-osmotic flow. Figure 7 shows the joint impacts of unequal zeta potential and the streaming potential on the flow pattern. As shown in the diagram, Ex is greater for harmonious wall zeta potentials (ξ_2^*= 1.0) than for asymmetric wall zeta potentials (ξ_2^*= 0.0). Furthermore, as κ increases, the streaming potential is shown to gradually decrease. This is due to the fact that (κ) is inversely related to the size of the EDL. It can be deduced that as $\kappa \to \infty$, the induced Ex→ 0.

Figure 8 demonstrates the combined actions of unequal zeta potential (ξ_2^*) and (κ) on the flow formation. It is demonstrated that the velocity gradient of a harmonious zeta potential (ξ_2^*= 1.0) is greater than that of an asymmetric zeta potential (ξ_2^*= 0.0).

Figure 9 exemplify the joint effects of (λ) and (ξ_2^*) on the velocity gradient. It is abundantly clear that, raising the levels of (λ) causes the fluid motion to expand, and this expansion is greater at (ξ_2^*= 1.0) than at (ξ_2^*= 0.0).

Table 1: Variation of pressure gradient, A for different values ofλ, Gre, Q and ξ where In=1.667, M=2, ε = 0.01, κ = 0.5, E_x=Γ= 2.0, $\xi = \xi_1^* = \xi_2^* = 1$

λ	Q	(ξ = 0, Gre=10) A	(ξ = 0, Gre=20) A	(ξ = 1, Gre=20) A
0.1		-27.9597	-7.1297	20.2053
0.2		-27.6299	-6.1070	22.1639
0.3	1	-27.3001	-5.0843	24.1226
0.4		-26.9703	-4.0615	26.0813
0.5		-26.6406	-3.0388	28.0400
0.1		-44.3980	-23.5681	3.7669
0.2		-44.0683	-22.5454	5.7256
0.3	2	-43.7385	-21.5226	7.6843
0.4		-43.4087	-20.4999	9.6429
0.5		-43.0789	-19.4772	11.6016

Table 2: Shows the critical values of Gre at the stationary plate y=1 for different flow parameters

λ	$\beta_v Kn$	(Q=1, κ = 2)	(Q=1, κ = 3)	(Q=2, κ = 5)
		Gre_1	Gre_1	Gre_1
0.1		3.9021	4.0488	5.2152
0.2		3.9770	4.1235	5.2892
0.3	0.0	4.0517	4.1981	5.3630
0.4		4.1263	4.2726	5.4367
0.5		4.2008	4.3470	5.5104
0.1		3.5730	3.6965	4.6878
0.2		3.6738	3.7971	4.7875
0.3	0.05	3.7744	3.8976	4.8871
0.4		3.8748	3.9979	4.9866
0.5		3.9751	4.0981	5.0858
0.1		3.2070	3.2884	3.8589
0.2		3.3214	3.4027	3.9726
0.3	0.1	3.4356	3.5168	4.0860
0.4		3.5495	3.6306	4.1992
0.5		3.6632	3.7442	4.3122

Table 3: Illustrates the skin friction (τ) at the cold plate y=0 and the heated plate y=1 for varying values of λ,Gre,$\beta_v Kn$ where In=1.667, M=2, e=0.01, κ = 0.5, Q=1, Ex=Γ= 2.0,$\xi = \xi_1^* = \xi_2^* = 1$

λ	($\beta_v Kn$=0.0, Gre=10)		($\beta_v Kn$=0.05, Gre=10)		($\beta_v Kn$=0.1, Gre=20)	
	τ_0	τ_1	τ_0	τ_1	τ_0	τ_1
0.1	81.6833	270.5131	73.8756	269.8140	135.7318	1038.7104
0.2	81.6954	271.2603	74.3365	270.7908	137.1795	1041.0561
0.3	81.7165	271.9611	74.7973	271.7603	138.6272	1043.3015
0.4	81.7332	272.6802	75.2581	272.7310	140.0749	1045.7004
0.5	81.7498	273.4016	75.7189	273.7101	141.5226	1048.0440

Table 4: The heat transfer coefficient Nu at the cold plate y=0 and the heated plate y=1 for varying values of λ,$\beta_v Kn$ and ξ where In=1.667, M=2, e=0.01

λ	($\beta_v Kn$=0.0, $\xi = -1$)		($\beta_v Kn$=0.05, $\xi = 0$)		($\beta_v Kn$=0.1, $\xi = 1$)	
	Nu_0	Nu_1	Nu_0	Nu_1	Nu_0	Nu_1
0.1	2.0673	2.3082	0.9448	0.7224	0.2077	0.2507
0.2	2.1363	2.6366	1.0326	0.5911	0.4319	0.6639
0.3	2.2069	2.9851	1.1204	0.4633	0.6726	1.0595
0.4	2.2792	3.3538	1.2083	0.3389	0.9297	1.6176
0.5	2.3532	3.7426	1.2963	0.2180	1.2033	2.2781

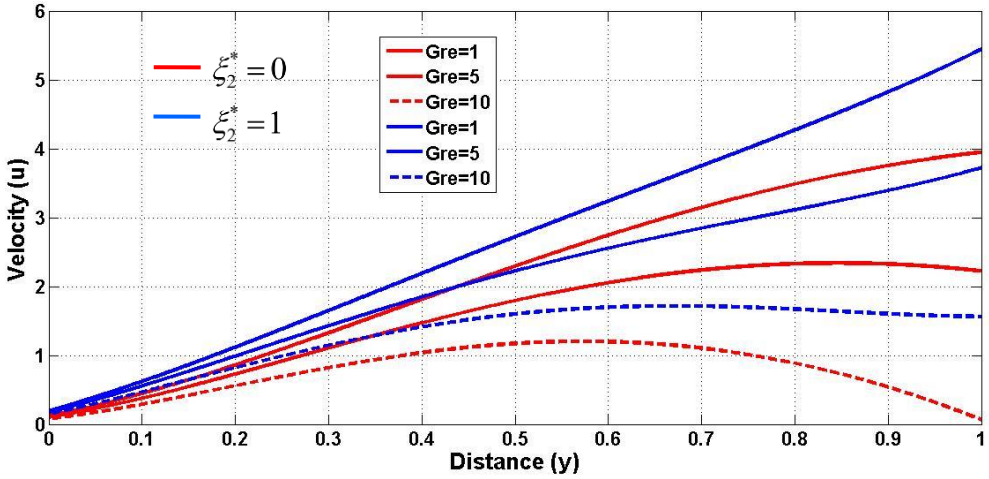

Figure 2: Result of Mixed convection Gre on velocity gradient for different (ξ_2^*)

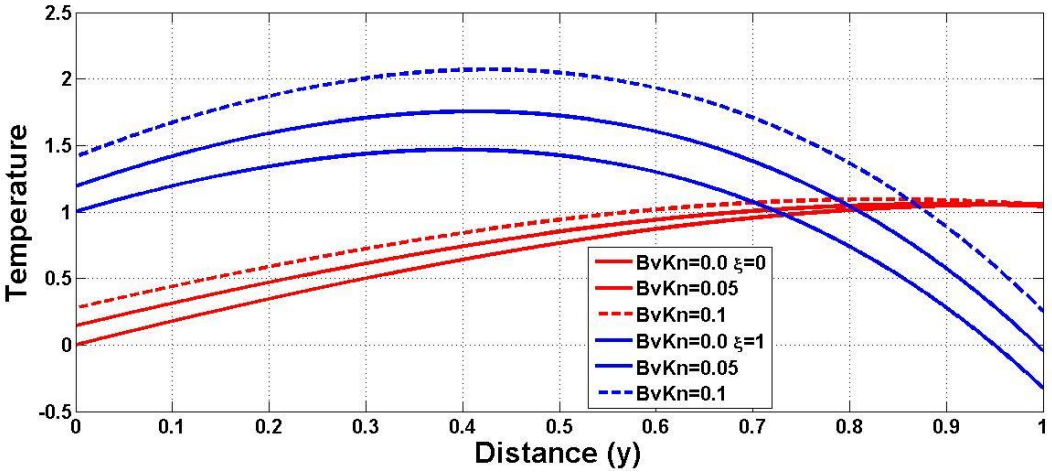

Figure 3: Result of $(\beta_v Kn)$ on temperature gradient

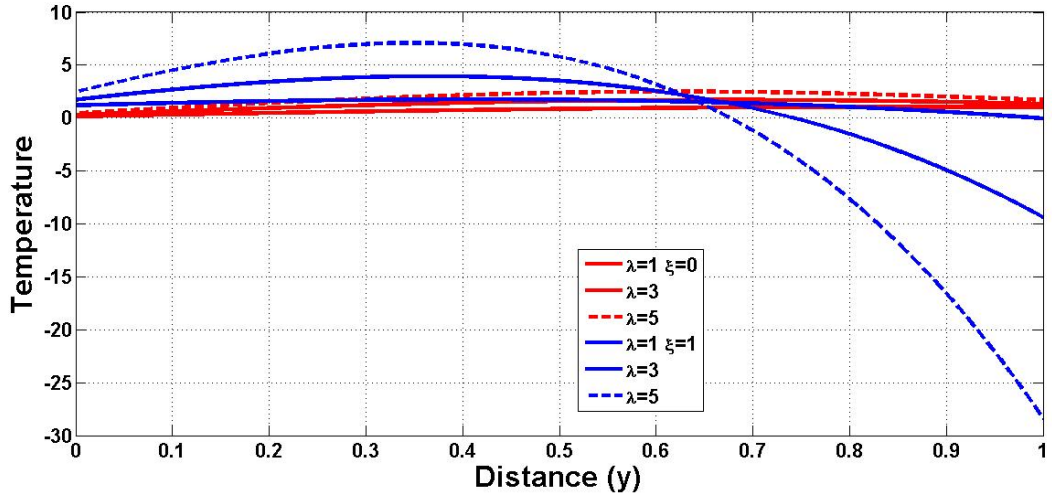

Figure 4: Result of λ on temperature gradient

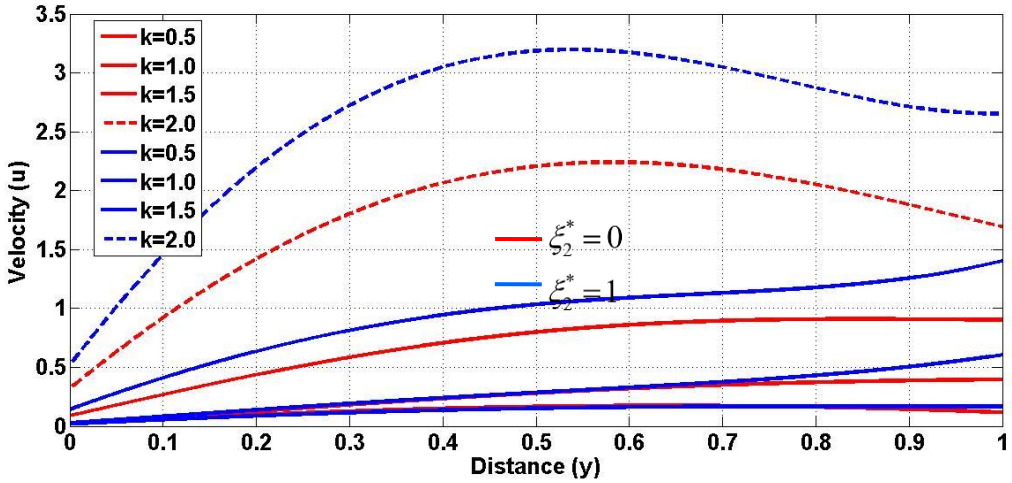

Figure 5: Result of κ on electrical potential for different (ξ_2^*)

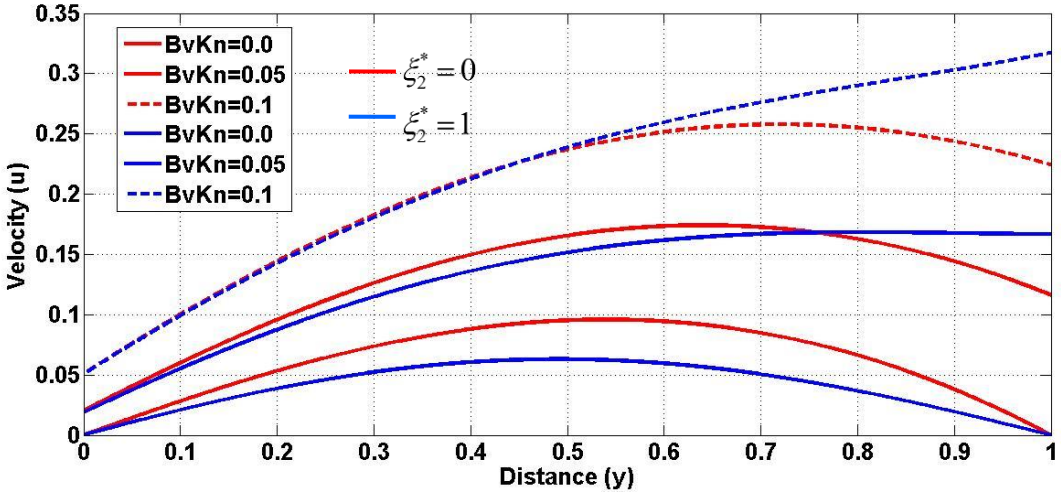

Figure 6: Result of $(\beta_v Kn)$ on velocity gradient for different (ξ_2^*)

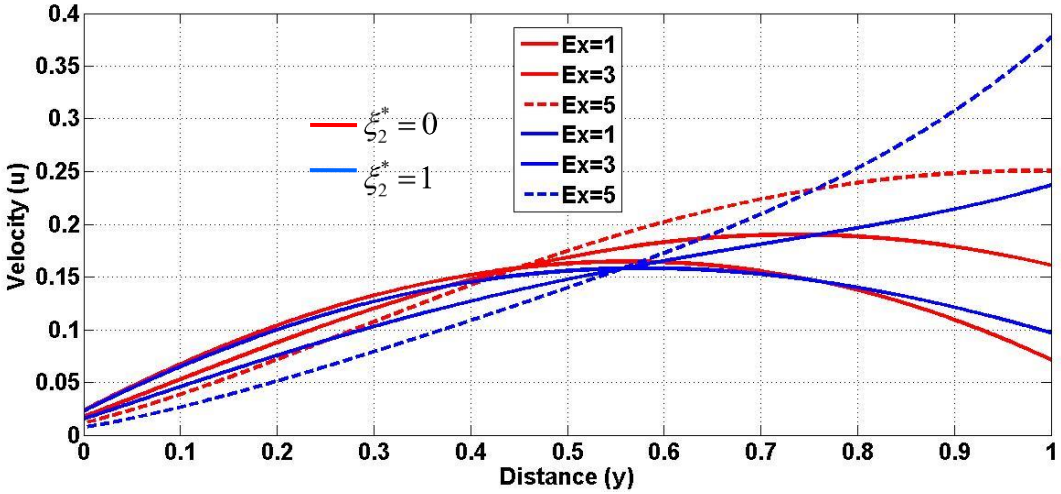

Figure 7: Result of Ex on velocity gradient for different (ξ_2^*)

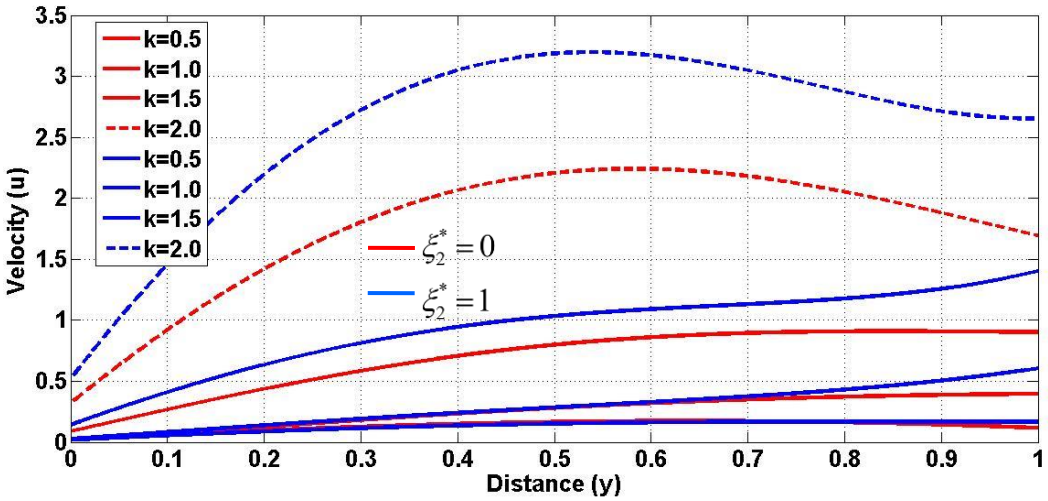

Figure 8: Result of κ on velocity gradient for different (ξ_2^*)

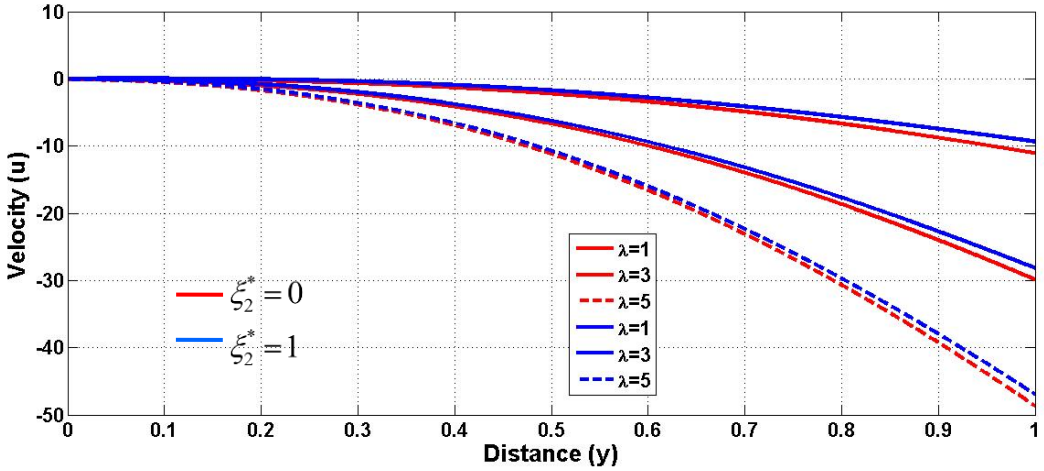

Figure 9: Result of λ on velocity gradient for different (ξ_2^*)

The deviations of the pressure gradient necessary to promote flow pattern is seen in Table 1. The table shows that as the chemical reactant parameters are increased, the pressure gradient decreases. This is to demonstrate that when chemical reactant energy is dissipated, a lower pressure gradient is needed to initiate flow. When natural convection dominates for a relatively small mass flux, a higher pressure gradient is necessary to operate against the flow.

The critical value of Gre at the cold plate (y = 1) is depicted in Table 2. It can be shown that increasing the rarefaction parameter results in decreased critical Gre levels. This is physically true because stronger energy is exerted in the fluid, necessitating a lower Gre value to eliminate plate boundary friction. The critical value of Gre grows as the chemical reactant parameter and mass flux are increased. Naturally, this is so because a strengthening of the mass flux lowers the convection current and makes the fluid to become thick, necessitating a higher Gre to eliminate boundary friction. A quick glance at the table reveals that each phenomenon that increases convection current necessitates a fall in Gre, whereas each quantity that weakens convection current necessitates an increase in Gre.

Table 3 depicts the fluid–plate interaction (skin friction). It is demonstrated that increasing the mixed convection and chemical reactant parameters reduces the sheer stress on both surfaces. However, as the rarefaction parameter rises on the hot plate, the skin friction increases, but a counter attribute is noticed on the cool plate. The increased frictional force at the heated plate is caused by an enhancement in the convection current, which causes an increase in fluid velocity, which increases skin friction.

The amount of heat transmission between the plates and the fluid is seen in Table 4. It is discovered that as chemical reaction parameters increase, the heat transfer coefficient reduces at the heated plate, whereas it increases at the cold plate. The diffusion of heat to the cold plate raises the thermal boundary layer thickness of the fluid at the cold plate, resulting in the improvement in the heat transfer coefficient. Increases in the wall ambient temperature differential ratio and rarefaction parameters diminish the heat transfer amount at the heated plate while increasing it at the cold plate, according to the findings.

Results Validation

In order to authenticate the correctness and precision of the current investigation, we compute the numerical comparison between the work of Jha et al. (2014a) and the present analysis for limiting case. The comparison confirms an excellent agreement for velocity and temperature gradients as portrayed in Table 5.

Table 5: Shows the numerical computations of comparison between the work of Jha et al. (2014a) with the current work for velocity and temperature for different $\xi = 0 and 1$ at $\beta_v Kn$=0.05, In=1.667, M=2, as Gre= 1 andλ=E$_x$=κ=A= 0

	y	Jha et al. (2014a) U(y)	Present work U(y)	Jha et al. (2014a) θ (y)	Present work θ (y)
$\xi = 0$	0.1	0.0233	0.0232	0.9251	0.9251
	0.2	0.0381	0.0380	0.9260	0.9260
	0.3	0.0508	0.0504	0.9268	0.9268
	0.4	0.0594	0.0592	0.9277	0.9277
	0.5	0.0660	0.0659	0.9286	0.9286
$\xi = 1$	0.1	0.0615	0.0614	1.0000	1.0000
	0.2	0.0934	0.0931	1.0000	1.0000
	0.3	0.1158	0.1148	1.0000	1.0000
	0.4	0.1285	0.1277	1.0000	1.0000
	0.5	0.1332	0.1320	1.0000	1.0000

CONCLUSION

A steady state magnetized flow of a chemically reacting fluid past a micro-channel was performed, with electro-osmotic effects taken into consideration. Employing the homotopy perturbation method (HPM), closed form expressions were used to estimate electric potential, temperature, velocity, skin friction, and the rate of heat transfer. The effects of major controlling factors such as Gre, λ, Ex, κ, $\beta_v Kn$, ξ and ξ_2^* parameters have been computed, and the results have been

represented with the aid of illustrative plots. The noteworthy outcomes of the present work are outlined below:

i. Growing fluid velocity and thermal gradient are noticed as the mixed convection and chemical reaction parameters increase at different ascending values of ξ.
ii. The highest electric potential is attained in the application of asymmetric zeta-potential on the micro-channel walls. Additionally, raising the Debye–Hückel parameter suppresses the electric potential.
iii. Heat transfer at the wall with asymmetric heating can be enhanced by considering the case of symmetric wall zeta potential.
iv. The skin-friction coefficient tends to increase at y=0 for mounting mixed convection parameter and chemical reaction parameters respectively, while a reverse case is envisaged at y=1.
v. The rate of heat transfer is significantly enhanced as the fluid is heated at y=0, with rising values of λ and ξ, whereas a contrast behavior is seen at y=1.
vi. When the pressure gradient, chemical reaction parameter and the electro-kinetics effects are ignored, as the mixed convection Gre=1, this current study reduces to the work of Jha *et al.* (2014a)
vii. The employed method (HPM) demonstrates an excellent potential in respect to accuracy and convergence for simulating flow.
viii. In the future, the impact of heat source/sink will be studied on this model.

REFERENCES

Ahmad, K. S., Jha, B. K. (2015). Computational methods of transient/steady natural convection flow of reactive viscous fluid in vertical porous pipe. Asian J. Math. Comput. Res. 2, 74–92

Ajibade, A. O., Umar, A. M. (2021). Effects of viscous dissipation on a steady mixed convection Couette flow of heat generating/absorbing fluid. Science Forum (J Pure Applied Sci). 21, 67-76. http://dx.doi.org/10.5455/sf.93898

Al-Nimr, M. A., Khadrawi, A. F. (2004). Thermal behavior of a stagnant gas confined in a horizontal microchannel as described by the dual-phase-lag heat conduction model. Int. J. Thermophy. 25, 1953–1964

Arulanandam, S., Li, D. (2000). Liquid transport in rectangular microchannels by electroosmotic pumping. Colloids Surf. A Physicochem. Eng. Asp. 161, 89–102.

Ayati, Z., Biazar, J. (2015). On the convergence of Homotopy Perturbation Method. J. Egyptian Math Soc. 23, 424-428

Buonomo, B., Manca, O. (2012). Natural Convection Flow in a Vertical Micro-Channel with Heated at Uniform Heat Flux. Int .J. Therm. Sci. 49, 1333-1344.

Chakraborty, J., Ray, S., Chakraborty, S. (2012). Role of streaming potential on pulsating mass flow rate control in combined electroosmotic and pressure-driven microfluidic devices. Electrophoresis 33, 419–425

Chen, C. K., Weng, H. C. (2005). Natural convection in a vertical micro-channel. J. Heat Transf. 127, 1053-1056.

Daniel, Y. S., Daniel, S. K. (2015). Effects of buoyancy and thermal radiation on MHD flow over a stretching porous sheet using homotopy analysis method. Alex. Eng. J. 54, 705–712.

Debye, P., Hückel, H. (1923). The theory of electrolytes. I. Lowering of freezing point and related phenomena. Phys. Z. 24, 185–206.

Frank- Kamenetskii D. A. (1969). Diffusion and Heat Transf , New York.

Hamza, M. M., Abdulsalam Shuaibu and Ahmad, S. K. (2022). Unsteady MHD free convection flow of an exothermic fluid in a convectively heated vertical channel filled with porous medium, Sci. Reports,12, 11989.

Hamza M. M., Shehu A., Muhammad I., Ojemeri G. and Shuaibu A. (2024a). Electrokinetically controlled mixed convective heat flow in a slit microchannel, Heat transfer Wiley, DOI: 10.1002/htj.23104, 1-20.

Hamza M. M., Shehu A., Muhammad I., Shuaibu A. and Ojemeri G. (2024b). Electro-kinetically free convective heat generation/absorption fluid in a slit micro-channel, *International Journal of Applied and Computational Mathematics,* https://doi.org/10.1007/s40819-024-01765-x

Hamza, M. M., Balarabe A. Y., Ibrahim M., Akpootu D. O. and Sheriff A. (2025). Transient fractional dusty fluid flow in a superhydrophobic microchannel, *European Physical Journal Plus,*140, 366, pp 1-17.

Hamza, M. M., Ojemeri, G., Abdulsalam, S. (2019). Mixed convection flow of viscous reactive fluids with thermal diffusion and radial magnetic field in a vertical porous annulus. Comput. math. mod. 30, 239-253. https://doi.org/10.1007/510598-019-09451-0

Hindebu, B., Makinde, O. D., Guta, L. (2022). Unsteady mixed convection flow of variable viscosity nanofluid in a micro-channel filled with a porous medium. Indian J Phys, 96, 1749-1766

Hunter, R. J. (1981). Zeta potential in Colloid Science: Principles and Applications. Academic Press, New York

Jamaludin, A., Naganthran, K., Nazar, R., Pop, I. (2020). MHD mixed convection stagnation-point flow of Cu-Al2O3/water hybrid nanofluid over a permeable stretching/shrinking surface with heat source/sink. Eur. J. Mech. Fluids 84, 71–80.

Jha B. K., Aina B. (2016). Role of induced magnetic field on MHD natural convection flow in vertical microchannel formed by two electrically non-conducting infinite vertical parallel plates. Alexandria Eng. J. 55, 2087-2097.

Jha B. K., Samaila, A. K., Ajibade, A. O. (2011a). Transient free-convective flow of reactive viscous fluid in a vertical channel. Int. Commun. Heat Mass Transf. 38, 633–637.

Jha, B. K, Samaila, A. K., Ajibade, A. O. (2011b). Transient free-convective flow of reactive viscous fluid in a vertical tube. Int. Commun. Heat Mass Transf. 54, 2880–2888

Jha, B. K. and Aina, B. (2015). Mathematical modeling and exact solution of steady fully developed mixed convection flow in a vertical micro-porous-annulus. J. AfrikaMatem-atika. 26, 1199-1213

Jha, B. K., Aina, B. Joseph, S. B. (2014b). Natural Convection Flow in vertical Micro-channel with Suction/Injection. J. Proc. Mech. Eng. 228, 171-180.

Jha, B. K., Aina, B., Ajiya, A. T. (2014a). MHD natural convection flow in a vertical parallel plate microchannel. Ain shams Eng. J. 6, 289-295.

Jha, B. K., Malgwi, P. B. (2019a). Hall current and ion – slip effects on free convection flow in a vertical microchannel with induced magnetic field. Heat Transf. Asian Res. 48, 1 – 19.

Jha, B. K., Malgwi, P. B., Aina. B. (2017). Hall effects on MHD natural convection flow in a vertical microchannel. Alexandria Eng. J, http://dx.doi.org/10.1016/j.aej.2017.01.038

Jha, B. K., Oni, M.O. (2018a). Transient natural convection flow between vertical concentric cylinders heated/cooled asymmetrically. Proc. I Mech E Part A J Power Energy. https://doi.org/10.1177/0957650918758743.

Jha, B. K., Oni, M.O. (2019b). Mathematical modeling of combined pressure driven and electro-kinetic effect in a channel with induced magnetic field: an exact solution. J. King Saud Univ. Sci. 31, 575–585. https://doi.org/10.1016/j.jksus.2018.10.009

Jha, B.K., Oni, M.O. (2019a). Natural convection flow in a vertical annulus with time-periodic thermal boundary conditions. Propul. Power Res. 8, 47–55

Liechty, B.C., Webb, B.W., Maynes, R. D. (2005). Convective heat transfer characteristics of electro-osmotically generated flow in microtubes at high wall potential. Int. J. Heat Mass Transf. 48, 2360–2371

Makinde O. D. (2008). Thermal criticality in viscous reactive flows through channels with a sliding wall: an exploitation of the Hermite–Pade approximation method. J. Math. Comput. Model. 47, 312–317.

Mala, G.H., Li, D., Dale, J.D. (1997). Heat transfer and fluid flow in microchannels. Int. J. Heat Mass Tranf.40 (13),3079–3088

Mandal, B., Bhattacharyya, k., Banerjee, A., kumarverma, A., Gautam A. k. (2020). MHD mixed convection on an inclined stretching plate in Darcy porous medium with soret effect and variable surface conditions. Nonlinear Eng., 9, 457-469.. https://doi.org/10.1515/nleng-2020-0029

Mukhopadhyay, A., Banerjee, S., Gupta, C. (2009). Fully developed hydrodynamic and thermal transport in combined pressure and electrokinetically driven flow in a microchannel with asymmetric boundary conditions. Int. J. Heat Mass Transf. 52, 2145–2154.

Muthuraj, R., Srinivas, S. (2010). Mixed convective heat and mass transfer in a vertical wavy channel with travelling thermal waves and porous medium. J. Comput. Math.Appl. 3516–3528 19.

Onwubuya I. O., Ojemeri G. and Uko M. A. (2024). Performance assessment of viscous dissipative fluid due to heat source/sink in a slit microchannel, *International Journal of Science for Global Sustainability,* 10(3), 139-151.

Ojemeri G., Hamza M. M., Tambuwal B H., Bello I. and Shuaibu A. (2023). Influence of Soret and radial magnetic field on natural convection of a chemically reactive fluid in an upright porous annulus, *UMYU Scientifica,* 2(3), pp. 108-120

Ojemeri G., Onwubuya I. O., Omokhuale E., Hussaini A. and Shuaibu A. (2024). Analytical investigation of Arrhenius kinetics with heat source/sink impacts along A heated superhydrophobic microchannel, *UMYU Scientifica,* 3(1), pp. 61-71.

Ojemeri, G. and Hamza, M. M. (2022). Heat transfer analysis of Arrhenius-controlled free convective hydromagnetic flow with heat generation/absorption effect in a micro-channel, Alexandria Eng. J., 61, pp. 12797-12811,

Ojemeri G. and Onwubuya I. O. (2023). Significance of viscous dissipation and porosity effects in a heated superhydrophobic microchannel, *Journal of Engineering Technology (JET),* 14(2), pp. 1-19

Ojemeri, G., Onwubuya I. O., Abdulsalam S. (2019). Effects of Soret and Radial magnetic field of a free convection slip flow in a viscous reactive fluid towards a vertical porous cylinder. Cont. J. Applied Sci, 14, 25-45. https://doi.org/10.5281/zenodo.265200.

Ojemeri G., Shuaibu A., Abubakar A. Y., Usman I. O. and Ahmad I. S. (2025). Dynamics of viscous Casson fluid on combined convection flow with exothermic chemical reaction in an upstanding tube, *Continental Journal of Aplied Sciences*, 20 (1): 61 – 79. https://doi.org/10.5281/zenodo.14925803

Oni, M. O. and Jha, B. K. (2019). Heat transfer analysis of mixed convection flow in a vertical microchannel with electrokinetic effect, *International Journal on Geomathematics*. https://doi.org/10.1007/s13137-020-00165-9

Oztop, H. F., Al-Salem, K., Pop, I. (2011). MHD mixed convection in a lid-driven cavity with corner heater. Int. J. Heat Mass Transf. 54, 3494–3504

Probstein, R.F. (1994). Physicochemical Hydrodynamics: An Introduction. Wiley, New York.

Reuss, F. F. (1809). Sur unnouveleffet de l'électricitégalvanique. Mém. Soc. Impér. Nat. Moscou. 2, 327–337

Weng, H. C., Chen, C. K. (2009). Drag reduction and heat transfer enhancement over a heated wall of a vertical annular microchannel. Int. J. Heat Mass Transf 52, 1075–1079

Yale I. D., Uchiri A. M. T., Hamza M. M. and Ojemeri G. (2023). Effect of viscous dissipative fluid in a slit microchannel with heated superhydrophobic surface, *Dutse Journal of Pure and Applied Sciences*, 9(3b), pp. 290-302.

Yang, C., Li, D. (1998). Analysis of electrokinetic effects on the liquid flow in rectangular microchannels. J. Colloids Surf. 143, 339–353.

APPENDIX

$$A_0 = \xi + \frac{BnKnIn(1-\xi)}{1+2BnKnIn}, A_1 = \frac{(1-\xi)}{1+2BnKnIn}, A_2 = BnKnInA_3$$

$$A_3 = \frac{\lambda BnKnIn(c_4 - c_5 + c_6) + \lambda(c_1 - c_2 + c_3)}{1+2BnKnIn}, A_4 = BnKnInA_5,$$

$$-BnKnIn(-c_{20} + c_{21} - c_{22} - c_{23} + c_{24} - c_{25} + c_{26} - c_{27} + c_{28} - c_{29} + c_{30} + c_{31})$$
$$+\lambda(4\lambda - 2e\lambda)(c_8 - c_9 + c_{10}) + c_{11}(4\lambda - 2e\lambda)(c_{12} - c_{13} + c_{14}) + c_{15}(4\lambda - 2e\lambda)$$

$$A_3 = \frac{-\lambda^2(c_{16} - c_{17} + c_{18}) - c_{19}}{1+2BnKnIn}$$

$$w1 = E_x\kappa^2\Gamma(\frac{D_0}{6} + \frac{D_1}{2}),\ w2 = \frac{Gr}{\mathrm{Re}}(\frac{A_0}{2} + \frac{A_1}{6}),\quad w3 = \beta_v KnE_x\kappa^2\Gamma(\frac{D_0}{6} + \frac{D_1}{2}),\quad w4 = \beta_v Kn\frac{Gr}{\mathrm{Re}}(\frac{A_0}{2} + \frac{A_1}{6}),$$

$$w5 = (1 + 2\beta_v kn),\qquad w6 = -w3 + w4 - w1 + w2,\qquad w7 = (\beta_v Kn + \frac{1}{2}), w8 = w6/w5, w9 = w7/w5,$$

$$w10 = M^2E_x\kappa^2\Gamma(\frac{D_0}{120} + \frac{D_1}{24}),\quad w11 = M^2\frac{Gr}{\mathrm{Re}}(\frac{A_0}{24} + \frac{A_1}{120}),\qquad w12 = M^2/24, w13 = M^2w8/6,$$

$$w14 = M^2w9/6, w15 = M^2\beta_v knw8/2, w16 = M^2\beta_v knw9/2,\quad w17 = E_x\kappa^4\Gamma[(\xi_2^* - \xi_1^*)\frac{1}{120} + \xi_1^*\frac{1}{24}]$$

$$w18 = E_x\kappa^2\Gamma(\frac{D_2}{6} + \frac{D_3}{2}),\qquad w19 = \lambda\frac{Gr}{\mathrm{Re}}[\frac{1}{24} + \frac{A_0}{24} + \frac{A_1}{120} + (2-e)(\frac{A_0^2}{24} + \frac{A_0A_1}{60} + \frac{A_1^2}{360})]$$

$$w20 = \frac{Gr}{\mathrm{Re}}(\frac{A_3}{6} + \frac{A_2}{2}),\quad w21 = BvknM^2E_x\kappa^2\Gamma(\frac{D_0}{24} + \frac{D_1}{6}),\qquad w22 = \beta_v KnM^2\frac{Gr}{\mathrm{Re}}(\frac{A_0}{6} + \frac{A_1}{24}),$$

$$w23 = BvknM^2/6,\quad w24 = BvknM^2w8/2,\ w25 = BvknM^2w9/2,\ w26 = Bvkn^2M^2w8,$$

$$w27 = Bvkn^2M^2w8,\quad w28 = BvknE_x\kappa^4\Gamma[(\xi_2^* - \xi_1^*)\frac{1}{24} + \xi_1^*\frac{1}{6}],\qquad w29 = BvknE_x\kappa^2\Gamma(\frac{D_2}{2} + D_3),$$

$$w30 = Bvkn\lambda\frac{Gr}{\mathrm{Re}}[\frac{1}{24} + \frac{A_0}{24} + \frac{A_1}{120} + (2-e)(\frac{A_0^2}{24} + \frac{A_0A_1}{60} + \frac{A_1^2}{360})], w31 = Bvkn\frac{Gr}{\mathrm{Re}}(\frac{A_3}{2} + A_2),$$

$$w32 = -w10 + w11 - w13 - w15 - w17 - w18 - w19 + w20 - w21 + w22 - w24 - w26 - w28 - w29 - w30 + w31,$$

$$w33 = w14 - w12 + w16 - w23 + w25 - w27,\quad w34 = w32/w5,\qquad w35 = w33/w5,$$

$$w36 = E_x\kappa^2\Gamma(\frac{D_0}{24} + \frac{D_1}{6}),\qquad w37 = \frac{Gr}{\mathrm{Re}}(\frac{A_0}{6} + \frac{A_1}{24}),\quad w38 = M^2E_x\kappa^2\Gamma(\frac{D_0}{720} + \frac{D_1}{120}),$$

$$w39 = M^2\frac{Gr}{\mathrm{Re}}(\frac{A_0}{120} + \frac{A_1}{720}),\quad w40 = M^2w8/24,\qquad w41 = M^2w9/24,\qquad w42 = M^2Bvknw8/6,$$

$$w43 = M^2Bvknw9/6,\ w44 = E_x\kappa^4\Gamma[(\xi_2^* - \xi_1^*)\frac{1}{720} + \xi_1^*\frac{1}{120}],\ w45 = E_x\kappa^2\Gamma(\frac{D_0}{24} + \frac{D_1}{6}),$$

$$w46 = \lambda\frac{Gr}{\mathrm{Re}}[\frac{1}{120} + \frac{A_0}{120} + \frac{A_1}{720} + (2-e)(\frac{A_0^2}{120} + \frac{A_0A_1}{360} + \frac{A_1^2}{2520})],\ w47 = \frac{Gr}{\mathrm{Re}}(\frac{A_3}{24} + \frac{A_2}{6}),$$

$$w48 = 1/6 - w9/2 - Bvknw9 + M^2/120 - w41 - w43 + w35/2 + Bvknw35,$$

$$w49 = -w36 + w37 - w8/2 - Bvknw8 - w8 - w39 - w40 - w42 - w44 - w45 - w46$$
$$+w47 - w34/2 - Bvknw34,\quad w50 = -w3/w5,\qquad w51 = \frac{1}{w5}\frac{Gr}{\mathrm{Re}}Bvkn(A_0 + \frac{A_1}{2}),$$

$$w52 = -w13/w5,\qquad w53 = \frac{1}{w5}\frac{Gr}{\mathrm{Re}}Bvkn(\frac{A_0}{2} + \frac{A_1}{6}),\ w54 = -w10/w5,$$

$$w55 = \frac{1}{w5}M^2\frac{Gr}{\mathrm{Re}}(\frac{A_0}{24} + \frac{A_1}{120}),\ w56 = (-w13 - w15 - w17 - w18)/w5,$$

$$w57 = \lambda\frac{1}{w5}\frac{Gr}{\mathrm{Re}}[\frac{1}{24} + \frac{A_0}{24} + \frac{A_1}{120} + (2-e)(\frac{A_0^2}{24} + \frac{A_0A_1}{60} + \frac{A_1^2}{360})],\quad w58 = \frac{1}{w5}\frac{Gr}{\mathrm{Re}}(\frac{A_3}{6} + \frac{A_2}{2}),$$

$$w59 = w21/w5,\qquad w60 = \frac{1}{w5}M^2Bvkn\frac{Gr}{\mathrm{Re}}(\frac{A_0}{6} + \frac{A_1}{24}),\qquad w61 = (-w24 - w26 - w28 - w29)/w5$$

$$w62 = \lambda\frac{1}{w5}\frac{Gr}{\mathrm{Re}}Bvkn[\frac{1}{6} + \frac{A_0}{6} + \frac{A_1}{24} + (2-e)(\frac{A_0^2}{6} + \frac{A_0A_1}{12} + \frac{A_1^2}{60})],\qquad w63 = \frac{1}{w5}Bvkn\frac{Gr}{\mathrm{Re}}(\frac{A_3}{2} + A_2),$$

$$w64 = w53 - w51 - w55 - w58 - w60 - \frac{Gr}{\mathrm{Re}}w62 + \frac{Gr}{\mathrm{Re}}w63,\qquad w65 = -w50 - w52 - \frac{dP}{dx}w9 - w54 + w56 - w57 - w59 + w61,$$

$$CC_1 = w8 - \frac{dP}{dx}w9,\qquad CC_2 = BvknCC_1,\qquad CC_3 = w34 + \frac{dP}{dx}w35,\ CC_4 = BvknCC_3$$

$$D_0 = \xi_2^* - \xi_1^*, D_1 = \xi_1^*, D_2 = -\kappa^2[(\xi_2^* - \xi_1^*)\frac{1}{6} + \xi_1^*\frac{1}{2}]$$

$$D_4 = -\kappa^4[(\xi_2^* - \xi_1^*)\frac{1}{120} + \xi_1^*\frac{1}{24}] - \kappa^2(\frac{D_2}{6})$$